HYPERSPECTRAL CODED APERTURE (HYCA): A NEW TECHNIQUE FOR HYPERSPECTRAL COMPRESSIVE SENSING

Gabriel Martín[1], *José M. Bioucas-Dias*[2] *and Antonio Plaza*[1]

[1]Hyperspectral Computing Laboratory, Department of Technology of Computers and Communications, University of Extremadura, E-10071 Caceres, Spain.
[2]Instituto de Telecomunicações, Instituto Superior Técnico, TULisbon, 1900-118, Lisbon, Portugal.

ABSTRACT

In this paper, we develop a new lossy compression framework for hyperspectral images, termed hyperspectral coded aperture (HYCA), which combines the ideas of spectral unmixing and compressive sensing. It takes advantage of two main properties of hyperspectral data, namely the high spatial correlation that can be observed in the data and the generally low number of endmembers needed in order to explain the data. In other words, our proposed approach intends to exploit the fact that the high dimensional hyperspectral data lives in a subspace of much lower dimension due to the mixing phenomenon. Our experimental results, conducted with synthetic hyperspectral data, indicate that the proposed approach represents a promising new strategy.

***Index Terms*—** Hyperspectral imaging, compressive sensing, spectral unmixing.

1. INTRODUCTION

Hyperspectral imaging allows an imaging spectrometer to collect hundreds of bands (at different wavelength channels) for the same area on the surface of the Earth [1]. For instance, the NASA Jet Propulsion Laboratory's Airborne Visible Infra-Red Imaging Spectrometer (AVIRIS) covers the wavelength region from 0.4 to 2.5 microns using 224 spectral channels, at nominal spectral resolution of 10 nanometers [2]. The resulting multidimensional data cube typically comprises several gigabytes per flight. Due to the extremely large volumes of data collected by imaging spectrometers, hyperspectral data compression has received considerable interest in recent years [3, 4]. These data are usually collected by a satellite or an airbone instrument and sent to a ground station on Earth for subsequent processing. Usually the bandwith connection between the satellite/airborne platform and the ground station is reduced, which limits the amount of data that can be transmitted. As a result, there is a clear need for (either lossless or lossy) hyperspectral data compression techniques that can be applied onboard the imaging instrument [5–7].

In addition to extremely large dimensionality, another problem in the analysis of hyperspectral data is the presence of mixed pixels [8], which result from insufficient spatial resolution or due to the presence of the mixture phenomenon at different scales. Mixed pixels can also result when distinct materials are combined into a homogeneus or intimate mixture. The spectra of the individual materials wich forms the mixed pixel are often called endmembers in the hyperspectral imaging literature [9]. Linear spectral unmixing is one of the more simple and widely used approaches for characterizing mixed pixels in hyperspectral data [10]. Let us assume that $\mathbf{Y} \in \mathbb{R}^{l \times n}$ is a hyperspectral image with l bands and n pixels. Under the linear mixture assumption, we can model the hyperspectral data as follows:

$$\mathbf{Y} = \mathbf{MA} + \mathbf{N}, \tag{1}$$

where $\mathbf{M} \in \mathbb{R}^{l \times p}$ is a matrix containing p endmembers and $\mathbf{A} \in \mathbb{R}^{p \times n}$ contains the abundance fractions asociated to each endmember in each pixel of the scene. Finally, $\mathbf{N} \in \mathbb{R}^{l \times n}$ is a matrix which represents the noise introduced in the model by the acquisition process. Over the last years, several techniques have been proposed for identifying the endmembers in $\mathbf{M}$ [11] and the abundances in $\mathbf{A}$ [10]. As a result, spectral unmixing has become an active research topic in recent years.

In this paper, we develop a new lossy compression framework for hyperspectral images, termed hyperspectral coded aperture (HYCA), which combines the ideas of spectral unmixing and compressive sensing [12–16]. It takes advantage of two main properties of hyperspectral data, namely the high spatial correlation that can be observed in the data and the generally low number of endmembers needed in matrix $\mathbf{M}$ in order to explain the data $\mathbf{Y}$. In other words, our proposed approach intends to exploit the fact that the high dimensional hyperspectral data lives in a subspace of much lower dimension due to the mixing phenomenon. In the following, we describe the newly developed approach and illustrate its potential using synthetic data.

2. METHOD DESCRIPTION

The HYCA algorithm is a lossy compresion algorithm for hyperspectral images. It is an algorithm of compressive sensing type which compresses the data on the adquisition process, then the compressed signal is sent to Earth and stored in compressed form. Later the original signal can be recovered with great fidelity by taking advantage of the fact that the hyperspectral data can be explained using a reduced set of spectral endmembers due to the mixing phenomenon and also exploits the high spatial correlation of the fractional abundances associated to the spectral endmembers. The algorithm can be briefly summarized as follows. First, we sub-sample the original hyperspectral data cube $\mathbf{Y}$ using a square window of size $m = ws \times ws$. For each window, we take each pixel in each position of the window and use it to generate a sub-sampled version of the original image

This work has been supported by the European Community's Marie Curie Research Training Networks Programme under contract MRTN-CT-2006-035927, Hyperspectral Imaging Network (HYPER-I-NET). Funding from the Portuguese Science and Technology Foundation, project PEst-OE/EEI/LA0008/2011, and from the Spanish Ministry of Science and Innovation (CEOS-SPAIN project, reference AYA2011-29334-C02-02) is also gratefully acknowledged.

$\mathbf{Y}$. For instance, if $ws = 2$, we obtain $m = 4$ sub-sampled versions of the original image so that $\mathbf{Y} = [\mathbf{Y}_1, \cdots, \mathbf{Y}_4]$, where the size in pixels of each sub-sampled version is $n/4$; if $ws = 3$, we obtain $m = 9$ sub-sampled versions of the original image so that $\mathbf{Y} = [\mathbf{Y}_1, \cdots, \mathbf{Y}_9]$, where the size in pixels of each sub-sampled version is $n/9$. As a result, depending on the size ws of the window we obtain set of m sub-sampled versions of the original image so that $\mathbf{Y} = [\mathbf{Y}_1, \mathbf{Y}_2, \cdots, \mathbf{Y}_m]$. In order to compress the original hyperspectral image and bring its dimensionality from l to q with $l > q$, thus achieving a compression ratio of l/q, we generate a random matrix $\mathbf{H} = [\mathbf{H}_1, \cdots, \mathbf{H}_m]$ where each $\{\mathbf{H}_i\}_{i=1}^m \in \mathbb{R}^{q \times l}$ is a random matrix. With these considerations in mind, we can compress the hyperspectral data $\mathbf{Y}$ by multiplying it by matrix $\mathbf{H}$, obtaining $\mathbf{HY} \in \mathbb{R}^{q \times n}$ as follows:

$$\mathbf{HY} = [\mathbf{H}_1\mathbf{Y}_1, \cdots, \mathbf{H}_m\mathbf{Y}_m] = \mathbf{HMA} \tag{2}$$

Let us now assume that $\mathbf{K} = \mathbf{HM} = [\mathbf{H}_1\mathbf{M}, \cdots, \mathbf{H}_m\mathbf{M}]$. If we have available the matrices $\mathbf{M}$ and $\mathbf{H}$, we can estimate $\mathbf{A}$ and decompress the transmitted, q-dimensional $\mathbf{HY}$ to obtain the original, l-dimensional image $\mathbf{Y}$ on the ground after data transmission. In order to do this, let $\|\mathbf{A}\|_F \equiv \sqrt{\text{trace}\{\mathbf{A}\mathbf{A}^T\}}$ be the Frobenius norm of $\mathbf{A}$. Since the abundance maps in hyperspectral images exhibit a lot of spatial correlation, we exploit this feature for estimating matrix $\mathbf{A}$ using the following optimization problem:

$$\begin{aligned} &\min_{\mathbf{A}} \frac{1}{2}\|\mathbf{Y} - \mathbf{KA}\|_F^2 + \lambda_{TV}\text{TV}(\mathbf{A}), \\ &\text{subject to } \ \mathbf{A} \geq 0, \end{aligned} \tag{3}$$

where:

$$\text{TV}(\mathbf{A}) \equiv \sum_{\{i,j\} \in \varepsilon} \|\mathbf{a}_i - \mathbf{a}_j\|_1 \tag{4}$$

is a vector extension of the non-isotropic TV [17], [18], which promotes piecewise constant (or smooth) transitions in the fractional abundance of the same endmember among neighboring pixels, and ε denotes the set of horizontal and vertical neighbors in the image. It should be noted that the optimization problem in Eq. (3), although convex, is very hard to solve owing to non-smooth terms and its huge dimensionality. To solve the problem in Eq. (3), we follow closely the methodology introduced in [19]. The core idea is to introduce a set of new variables per regularizer and then use the alternating direction method of multipliers (ADMM) [20] to solve the resulting constrained optimization problem. By a careful choice of the new variables, the initial problem is converted into a sequence of much simpler problems. With this in mind, an equivalent way of writing the optimization problem in Eq. (3) is:

$$\min_{\mathbf{A}} \frac{1}{2}\|\mathbf{Y} - \mathbf{KA}\|_F^2 + \lambda_{TV}\|\mathbf{LA}\|_{1,1} + \iota_{R+}(\mathbf{A}), \tag{5}$$

where $\mathbf{L} \equiv [{\mathbf{L_h}}^T {\mathbf{L_v}}^T]^T$ is a linear operator computing the horizontal and vertical differences between the components of $\mathbf{A}$ corresponding to neighboring pixels and $\iota_{R+}(\mathbf{A}) = \sum_{i=1}^n \iota_{R+}(\mathbf{a}_i)$ is the indicator function ($\mathbf{a}_i$ represents the i-th column of $\mathbf{A}$ and $\iota_{R+}(\mathbf{a}_i)$ is zero if $\mathbf{a}_i$ belongs to the nonnegative orthant and $+\infty$ otherwise). Given the objective function in Eq. (5), we write the following (constrained) equivalent formulation:

$$\begin{aligned} \min_{\mathbf{A},\mathbf{V}_1,\mathbf{V}_2,\mathbf{V}_3,\mathbf{V}_4} \quad & \frac{1}{2}||\mathbf{Y} - \mathbf{KV}_1||_F^2 + \iota_{R+}(\mathbf{V}_2) + \lambda_{TV}||(\mathbf{V}_3, \mathbf{V}_4)||_1 \\ \text{subject to} \quad & \mathbf{A} = \mathbf{V}_1 \\ & \mathbf{A} = \mathbf{V}_2 \\ & \mathbf{LA} = (\mathbf{V}_3, \mathbf{V}_4) \end{aligned} \tag{6}$$

3. EXPERIMENTAL RESULTS

In this section, we illustrate the proposed HYCA approach using synthetic hyperspectral images generated from spectral signatures randomly selected from the United States Geological Survey (USGS)[1]. The simulated images consist of a set of 5×5 squares of 10×10 pixels each one, for a total size of 110×110 pixels. The first row of squares contains the endmembers, the second row contains mixtures of two endmembers, the third row contains mixtures of three endmembers, and so on. Zero-mean Gaussian noise was added to the synthetic scenes in different signal to noise ratios (SNRs) – 30dB, 50dB and 70dB– to simulate contributions from ambient and instrumental sources, following the procedure described in [21]. For illustrative purposes, Fig. 1 displays the ground-truth abundances maps used for generating the simulated imagery.

In order to evaluate the performance of the HYCO method, we used as performance discriminator the root mean square error (RMSE) between the original image and the reconstructed image after data compression and decompression. In our experiments, we used a window size of $ws = 2$, so that $m = 4$. Here, the number of endmembers was set to $p = 5$ based on the ground-truth information. For the synthetic image without noise, we used the USGS endmembers to form matrix $\mathbf{M}$ while in the noisy cases we derived the endmembers using the vertex component analysis (VCA) algorithm [21]. In this experiment, we bring the dimensionality of the original hyperspectral image from $l = 224$ to $q = 3$, thus achieving a compression ratio of $l/q = 74.67$. Table 3 shows the RMSE between the original and the reconstructed images. Here, we performed 10 Monte-Carlo runs for each case as the generation of matrix $\mathbf{H}$ is random and reported the average value obtained (plus/minus the standard deviation) in Table 3. In all cases, we optimized the λ_{TV} parameter empirically. As shown by Table 3, the RMSE values are consistently very low, with very small standard deviation across the conducted Monte-Carlo runs. For illustrative purposes, Fig. 2(a) shows one of the spectral bands of the original synthetic image with SNR=∞ (specifically, band number 50) while Fig. 2(e) shows the same band in the image after compression and decompression. Similarly, the image pairs in Figs. 2(b,f), Fig. 2(c,g) and Fig. 2(d,h) show the same band in the original and reconstructed image for SNR values of 70dB, 50dB and 30dB, respectively. Even in high noise scenarios, the quality of the decompressed image is quite high, despite the use of a very high compression ratio above 70. Despite the fact that the results obtained are very encouraging, further experimentation with real hyperspectral scenes is highly desirable. These will be conducted in future work.

4. REFERENCES

[1] A. F. H. Goetz, G. Vane, J. E. Solomon, and B. N. Rock, "Imaging spectrometry for Earth remote sensing," *Science*, vol.

[1] http://speclab.cr.usgs.gov/spectral-lib.html

(a) Endmember #1 (b) Endmember #2 (c) Endmember #3 (d) Endmember #4 (e) Endmember #5

Fig. 1. True abundance maps of endmembers in the synthetic hyperspectral data.

.

Table 1. Average (plus/minus standard deviation) of the reconstruction RMSE between the original and the reconstructed images after compression/decompression (for different SNR values) after 10 Monte-Carlo runs.

SNR=30dB	SNR=50dB	SNR=70dB	SNR=∞
0.01820 ± 0.00095	0.0025 ± 0.00031	0.00055 ± 0.00020	0.00030 ± 0.00025

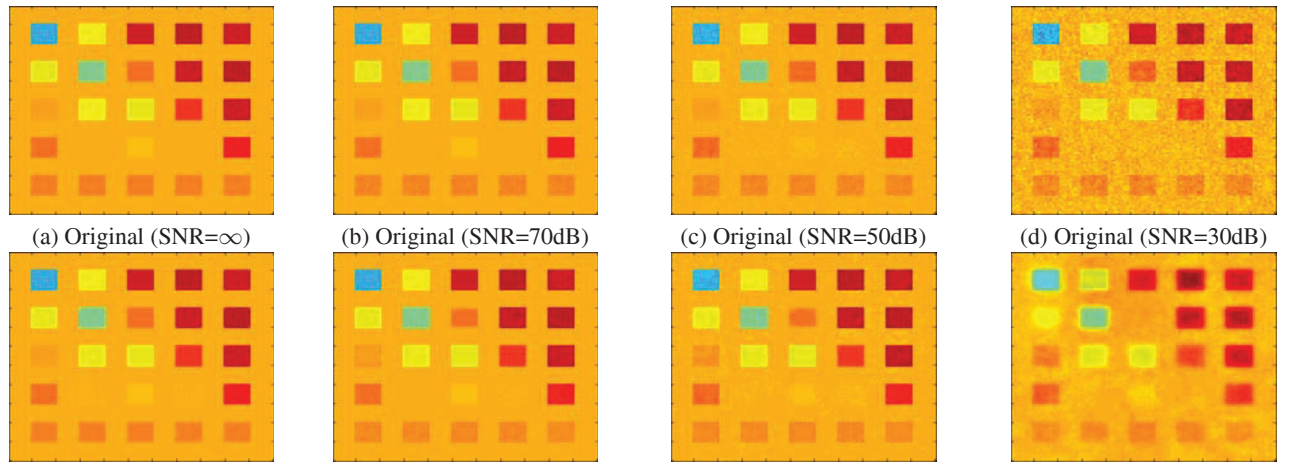

(a) Original (SNR=∞) (b) Original (SNR=70dB) (c) Original (SNR=50dB) (d) Original (SNR=30dB)

(e) Decompressed (SNR=∞) (f) Decompressed (SNR=70dB) (g) Decompressed (SNR=50dB) (h) Decompressed (SNR=30dB)

Fig. 2. Band 50 of the synthetic hyperspectral image (top row) and the decompressed image (bottom row) for different SNR values.

228, pp. 1147–1153, 1985.

[2] R. O. Green, M. L. Eastwood, C. M. Sarture, T. G. Chrien, M. Aronsson, B. J. Chippendale, J. A. Faust, B. E. Pavri, C. J. Chovit, M. Solis, et al., "Imaging spectroscopy and the airborne visible/infrared imaging spectrometer (AVIRIS)," *Remote Sensing of Environment*, vol. 65, no. 3, pp. 227–248, 1998.

[3] G. Motta, F. Rizzo, and J. A. Storer, *Hyperspectral data compression*, Berlin: Springer, 2006.

[4] Bormin Huang, *Satellite data compression*, Berlin: Springer, 2011.

[5] Qian Du and James E. Fowler, "Low-complexity principal component analysis for hyperspectral image compression," *International Journal of High Performance Computing Applications*, vol. 22, pp. 273–286, 2009.

[6] Changhe Song, Yunsong Li, and Bormin Huang, "A GPU-accelerated wavelet decompression system with SPIHT and Reed-Solomon decoding for satellite images," *IEEE Journal of Selected Topics in Applied Earth Observations and Remote Sensing*, vol. 4, no. 3, 2011.

[7] Shih-Chieh Wei and Bormin Huang, "GPU acceleration of predictive partitioned vector quantization for ultraspectral sounder data compression," *IEEE Journal of Selected Topics in Applied Earth Observations and Remote Sensing*, vol. 4, no. 3, 2011.

[8] N. Keshava and J. F. Mustard, "Spectral unmixing," *IEEE Signal Processing Magazine*, vol. 19, no. 1, pp. 44–57, 2002.

[9] A. Plaza, P. Martinez, R. Perez, and J. Plaza, "A quantitative and comparative analysis of endmember extraction algorithms from hyperspectral data," *IEEE Transactions on Geoscience and Remote Sensing*, vol. 42, no. 3, pp. 650–663, 2004.

[10] A. Plaza, Q. Du, J. Bioucas-Dias, X. Jia, and F. Kruse, "Foreword to the special issue on spectral unmixing of remotely sensed data," *IEEE Transactions on Geoscience and Remote Sensing*, vol. 49, no. 11, pp. 4103–4110, 2011.

[11] Q. Du, N. Raksuntorn, N. H. Younan, and R. L. King, "End-member extraction for hyperspectral image analysis," *Applied Optics*, vol. 47, pp. 77–84, 2008.

[12] D. Donoho, "Compressed sensing," *IEEE Transactions on Information Theory*, pp. 1289–1306, 2006.

[13] M. Afonso, J. Bioucas-Dias, and M. Figueiredo, "A fast algorithm for the constrained formulation of compressive image reconstruction and other linear inverse problems," *Proceedings of the IEEE International Conference on Acoustics, Speech, and Signal Processing*, vol. 1, pp. 4034–4037, 2010.

[14] Z. Guo, T. Wittman, and S. Osher, "L1 unmixing and its application to hyperspectral image enhancement," *Proceedings SPIE Conference on Algorithms and Tech- nologies for Multispectral, Hyperspectral, and Ultraspectral Imagery*, 2009.

[15] C. Li, T. Sun, K. Kelly, and Y. Zhang, "A compressive sensing and unmixing scheme for hyperspectral data processing," *IEEE Transactions on Image Processing*, , no. 99, pp. 1–1, 2011.

[16] Q. Zhang, R. Plemmons, D. Kittle, D. Brady, and S. Prasad, "Joint segmentation and reconstruction of hyperspectral data with compressed measurements," *Applied Optics*, vol. 50, no. 22, pp. 4417–4435, 2011.

[17] L. Rudin, S. Osher, and E. Fatemi, "Nonlinear total variation based noise removal algorithms," *Physica D: Nonlinear Phenomena*, vol. 60, no. 1-4, pp. 259–268, 1992.

[18] A. Chambolle, "An algorithm for total variation minimization and applications," *Journal of Mathematical Imaging and Vision*, vol. 20, pp. 89–97, 2004.

[19] M. Afonso, J. Bioucas-Dias, and M. Figueiredo, "An augmented Lagrangian approach to the constrained optimization formulation of imaging inverse problems," *IEEE Transactions on Image Processing*, vol. 20, no. 3, pp. 681 –695, 2011.

[20] J. Eckstein and D. Bertsekas, "On the Douglas-Rachford splitting method and the proximal point algorithm for maximal monotone operators," *Mathematical Programming*, vol. 5, pp. 293–318, 1992.

[21] J. M. P. Nascimento and J. M. Bioucas-Dias, "Vertex component analysis: A fast algorithm to unmix hyperspectral data," *IEEE Transactions on Geoscience and Remote Sensing*, vol. 43, no. 4, pp. 898–910, 2005.